Rapid formation of zinc oxide nanosheets on titanium dioxide nanotubes through electrochemical method

S. W. NG*, F. K. YAM, Z. HASSAN
Nano-Optoelectronics Research and Technology Laboratory School of Physics, Universiti Sains Malaysia, 11800 Penang, Malaysia

Highly ordered TiO_2 nanotubes array have been prepared through anodization process in fluoride based electrolyte. ZnO nanosheets have been grown on the as-anodized TiO_2 nanotubes through rapid electrodeposition process in ethanolic $Zn(NO_3)_2$ electrolyte and the identical procedures have been repeated on Zn foil for comparison. No extreme temperature and only low applied potential were required in the process of fabricating ZnO nanosheets. The growth manner of the ZnO nanosheets whereby the nanosheets favoured to be in near spherical cluster instead of individual sheets has been ascribed to the minimum surface energy. The dimensions of the cluster and individual nanosheet have been analyzed through a large population to evaluate the average sizes. X-ray diffraction and Raman measurement results supported the suggested chemical reactions for the formation of nanosheets and proved that the nanosheets are comprised of ZnO. It has been discovered that the ZnO nanosheets grown on both TiO_2 nanotubes and Zn foil demonstrated similar physical properties, with additional advantages on the use of TiO_2 nanotubes template.

(Received August 14, 2014; accepted October 28, 2015)

Keywords: Hybrid structure, Electrodeposition, Formation mechanism

1. Introduction

Zinc oxide (ZnO) is a wide and direct semiconductor with optical bandgap of 3.37 eV while titanium dioxide (TiO_2) is a n-type indirect semiconductor with optical bandgap between 3.0–3.2 eV depending on its crystal phases. Both metal oxides share potential applications in optoelectronic devices, including solar cells, chemical sensors, gas sensors and storage technology [1–4].

As compared to bulk solids or thin films, nanostructured materials exhibit unique physical and chemical properties due to their large surface-to-volume ratio. Zinc (Zn), by nature, is easy to transform into diverse ZnO nanostructures such as nanowire [3], nanoneedle [5,6] and nanobelts [5,7,8]. Commonly reported ZnO nanostructures fabrication methods are thermal evaporation [2,8], hydrothermal [9], electrochemical [10], chemical vapour deposition (CVD) [11]. While hydrothermal [12], seeded-growth mechanism [13], electrochemical [14] and template-assisted sol-gel [15, 16] are widely employed to fabricate TiO_2 nanostructures such as nanowires [4], nanotubes [14] and nanofibers [17, 18]. For both ZnO and TiO_2, electrochemical method has gained interest of researchers due to its low cost and simple experimental setup. It is commonly reported that metal oxide nanostructures i.e. ZnO or TiO_2 nanostructures can be obtained through anodization of the parent metal, i.e. Zn [19] or Ti [20, 21], respectively. Depending on the applications, other templates for instance porous anodic alumina [15], silicon substrates [22] and indium-tin-oxide (ITO) transparent glass substrates [23] may be utilized to fabricate metal oxide nanostructures.

From thin film to nanostructure, efforts have been given to merge ZnO and TiO_2 regardless the orientation and the fabrication method. Shi et al. reported multilayer thin film of TiO_2/ZnO and ZnO/TiO_2 and observed a rare violet luminescence due to the interface traps between extra grain boundary defects of ZnO and TiO_2 layers [24]. Xu et al. studied ZnO thin film covered by TiO_2 nanoparticles and observed an enhanced ultraviolet (UV) emission which suppressed green emission [25]. This was attributed to the atomic interdiffusion between TiO_2 nanoparticles and ZnO layer causing interface defects and internal point defects. Zou et al. fabricated ZnO/TiO_2 bottle brush-like heterostructure and discovered enhanced photocatalytic activity with appropriate TiO_2 length and density [26].

In this work, ZnO nanosheets on highly ordered TiO_2 nanotube arrays was fabricated through two electrochemical steps, firstly anodization to obtain TiO_2 nanotube and subsequently electrodeposition to obtain ZnO nanosheets. These two metal oxide nanostructures were incorporated to study its structural and vibrational properties in hope to provide an insight to integrate two or more metal oxide nanomaterials in future studies for different applications [14, 26–28].

2. Experimental

Highly ordered TiO_2 nanotubes were prepared through anodization method as reported earlier [29]. Briefly, Ti foil (purchased from Strem chemicals) of 99.7% purity with thickness 0.127 mm was degreased by alkaline solution and rinsed in deionized (DI) water. The Ti foil was served as anode while platinum (Pt) rod as cathode. Both were

anodized under constant potential of 40 V for 30 mins under room temperature. A mixture of ethylene glycol (EG) and hydrogen peroxide (H_2O_2) in 9:1 volume ratio and 0.3 wt% of ammonia fluoride (NH_4F) formed the electrolyte. The TiO_2 nanotubes sample obtained through anodization process was rinsed with DI water and dried under air ambient.

The as-anodized TiO_2 nanotubes was then served as template for electrodeposition process. The electrolyte consisted of ethanol and zinc nitrate hexahydrate ($Zn(NO_3)_2.6H_2O$) in 1:1 volume ratio. A constant potential of –4 V was applied for 2 mins under room temperature. Finally, the ZnO nanosheets grown on TiO_2 nanotubes was dried under air ambient. As a comparison, identical electrodeposition was repeated on a degreased Zn foil (purchased from Strem chemicals) of 99.98% purity.

The surface morphology of TiO_2 nanotubes, ZnO nanosheets deposited TiO_2 nanotubes were characterized by transmission electron microscopy (TEM) (FEI CM 12). All samples were then characterized by field emission scanning electron microscopy (FE-SEM) (Zeiss Leo Supra 50VP) and qualitative analysis were done by energy dispersive X-ray spectroscopy (EDX) attached to FE-SEM. The structural characteristic of the samples was obtained by high resolution X-ray diffractometer (HR-XRD) (PANalytical X'pert PRO MRD PW3040) with $CuK_{\alpha 1}$ source of 0.154 nm wavelength. Raman spectra were obtained by Raman spectroscopy system (Jobin Yvon hr 800 UV) at room temperature. Ar^+ laser source 20 mW at 514.5 nm was employed to examine the vibrational properties. Prior to HR-XRD and Raman measurements, the samples were calcined at 500 ^{o}C under air ambient for 1 h.

3 Results and discussion

3.1 Morphology

For comparison of the tubes morphology of TiO_2 nanotubes before and after deposition of ZnO nanosheets, a FE-SEM image of the as-anodized TiO_2 nanotubes is presented in Fig. 1 (a). It is noticed that the nanotubes are homogeneous with perfect circular rims, standing independently and having self-organized individual tube wall of approximately 10 nm. The individual tube is connected with neighbouring tubes by the ripples surrounding the outer tube wall as seen in TEM image in Fig. 1 (b).

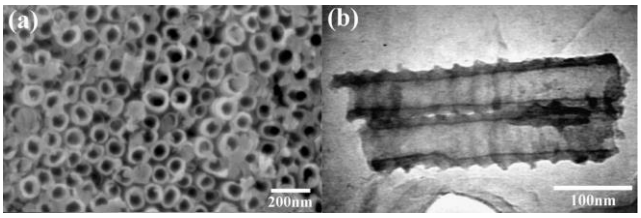

Fig. 1. The as-anodized bare TiO_2 nanotubes with definite tube wall, tube diameter approximately 100 nm (a) FE-SEM image and (b) TEM image.

The as-anodized nanotubes were then undergone electrodeposition process to fabricate ZnO nanostructures on top of the TiO_2 nanotubes. Within merely 2 mins, spherical clusters of different sizes were rapidly formed and covered the entire surface of TiO_2 nanotubes as presented in panoramic morphologies in Fig. 2. Higher magnification images in Figs. 2 (b)-(c) evidenced that ZnO nanosheets were concealed in the clusters. TEM image in Fig. 2 (d) revealed that the hollow area of TiO_2 nanotubes was partially filled by excess ZnO, and the excess ZnO was believed to fall into the tiny spaces between individual tube walls and being trapped by the ripples connecting the tube walls. This can be observed from the non-uniform and thicker ripples of TiO_2 nanotubes in Fig. 2 (d) which is not observed in the outer tube surface prior to electrodeposition as shown in Fig. 1 (b).

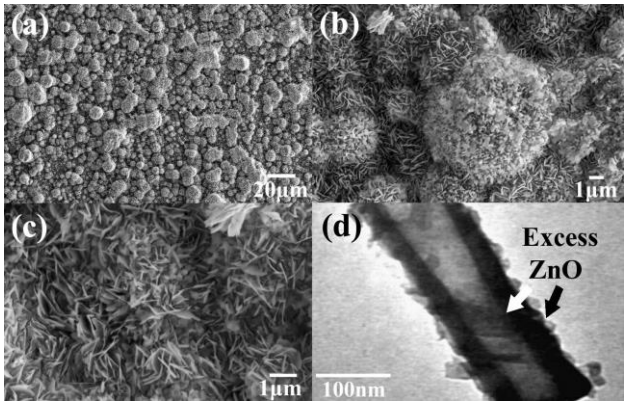

Fig. 2. (a)-(c) ZnO nanosheets concealed in the clusters on top of TiO_2 nanotubes surface, at different magnifications. (d) TEM image of hollow part TiO_2 nanotubes partially filled by ZnO. Excess ZnO trapped between tube walls is shown by uneven and thicker tube ripples.

In order to investigate the influence of TiO_2 nanotubes template to the growth of ZnO nanostructure, the identical procedure of fabricating ZnO nanosheets was repeated on pure Zn foil. Fig. 3 shows a similar nanostructure. The fine layer of the greyish-white ZnO nanosheets was easily self-detached into powdery form, imparting uneven bare Zn surface given in the inset of Fig. 3 (a). Note that this was not observed in the case of TiO_2 nanotubes. Careful handling procedures were thus required for ZnO nanosheets on Zn foil. Refer to the higher magnification image, the nanosheets grown on pure Zn foil was larger in size than that on TiO_2 nanotubes. The distribution of the actual size of nanosheets grown on two different substrates will be further analyzed in the later part of this section.

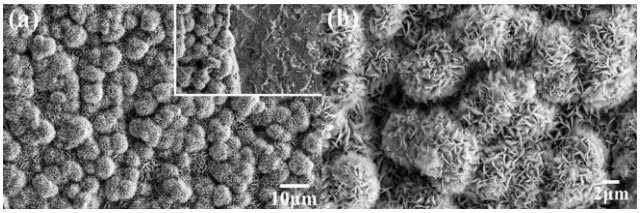

Fig. 3. (a)-(b) ZnO nanosheets concealed in the clusters on top of Zn foil, at different magnifications, inset in (a) shows bare Zn surface after the removal of ZnO nanosheets layer.

The preference to form nanosheets clusters instead of separate nanosheets contradicts to several cases. Generally, the ZnO nanosheets obtained through electrochemical method in other works had scattered profiles on the substrate surface. Closely packed ZnO nanostructures can only be achieved in the exception of prolonging electrodeposition time and changing the electrolyte temperature to extreme conditions. Zhang et al. [28] reported similar electrodeposition of 60 mins carried out in aqueous based $Zn(NO_3)_2$ electrolyte and the ZnO rods were 100–200 nm. Based on their observations, it can be deduced that the use of concentrated ethanol based electrolyte in this project has promoted the growth rate of ZnO nanosheets. The suggested chemical reactions occurred during the process are presented in equations 1 – 5 [1, 30].

$$Zn(NO_3)_2 \rightarrow Zn^{2+} + 2NO_3^- \quad (1)$$

$$NO_3^- + H_2O + 2e^- \rightarrow NO_2^- + 2OH^- \quad (2)$$

$$Zn^{2+} + 2OH^- \rightarrow Zn(OH)_2 \quad (3)$$

$$Zn(OH)_2 \rightarrow ZnO + H_2O \quad (4)$$

The overall reaction is given by

$$Zn^{2+} + NO_3^- + 2e^- \rightarrow ZnO + NO_2^- \quad (5)$$

In regard to the FE-SEM images in Figs. 2 and 3, the diameter of the spherical clusters and the length of individual ZnO nanosheet, grown on both TiO_2 nanotubes and Zn foil were analyzed over a large population. The distributions are presented in Fig. 4. The spherical clusters were randomly selected, and for each cluster, a number of ZnO nanosheets were randomly selected. The clusters diameter grown on TiO_2 nanotubes and Zn foil varied from 1–17 μm and 4–9.5 μm across, respectively. The negatively-skewed distribution in Fig. 4 (a) indicates that the ZnO nanosheets on TiO_2 nanotubes prefer to form a smaller scale cluster, especially in the range of 3–5 μm diameter. Approaching a symmetrical distribution in Fig. 4 (c), indicates that ZnO nanosheets on Zn foil tend to grow in the range of 6–7.5 μm diameter. Evidently, ZnO nanosheet clusters grown on TiO_2 nanotubes is smaller in diameter size in comparison to the clusters on Zn foil, which is in good agreement with the initial observation.

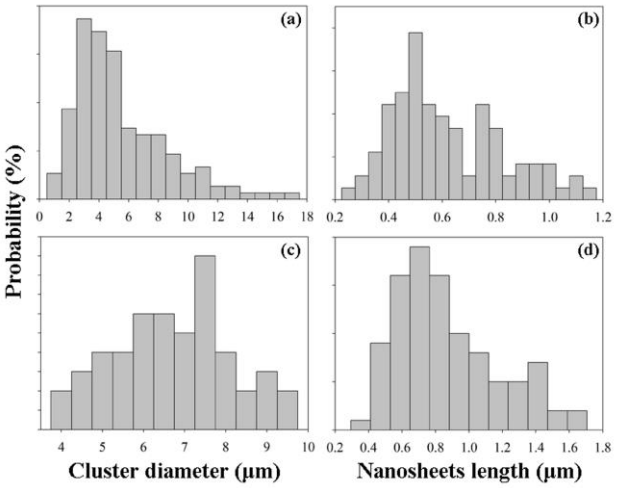

Fig. 4. Distribution of spherical clusters diameter and individual nanosheets length of ZnO nanosheets grown on different substrates (a),(b) on TiO_2 nanotubes, (c),(d) on Zn foil. Each division on the probability axis represents 5%

Lengthwise, nanosheets on TiO_2 nanotubes cover a broad range from 0.25–1.15 μm. Two prominent peaks positioned at 0.5 and 0.75 μm are observed from the distribution in Fig. 4 (b). Generally, the distribution is negatively-skewed, suggests that the growth of ZnO nanosheets is directed to shorter length. The same trend is demonstrated by the nanosheets on Zn foil, ranging from 0.35–1.65 μm in Fig. 4 (d). It is important to note that the average size of nanosheets on TiO_2 nanotubes and Zn foil are 0.62 and 0.87 μm respectively. Comparing the size of ZnO nanosheets grown on galvanized-steel through anodization method by Ng et al. [31], the shortest average length was 1.23 μm, in current work we have made a significant advancement. Half of the nanosheet size, i.e. 0.62 μm on average can be achieved with the requirement of relatively short duration, i.e. 2 mins compared to Ng et al. at 60 mins. In addition, current work requires only 2 V of applied potential but Ng et al. at 10 V. The orientation of nanosheets is random with their sharp tips oriented at no particular direction based on the observation in Figs. 2 (c) and 3 (b).

Analysis on the mean physical size of ZnO nanosheets grown on TiO_2 nanotubes and Zn foil is presented in Table 1. The number of nanosheets per cluster surface area was calculated in the basis of two assumptions: 1. Each cluster is treated as a perfect sphere (circle as seen on two dimensional plane). 2. ZnO nanosheets are evenly distributed on the entire surface of the spherical cluster. Note that TiO_2 nanotubes surface has the capacity to accommodate nanosheets double to that of Zn foil surface. Hence, TiO_2 nanotubes is a preferable template to fabricate ZnO nanosheets as more quantity of individual

nanosheets could be grown with the identical experiment parameters. The increase of quantity of individual nanosheet increases the surface area-to-volume ratio of the entire nanostructure which potentially enhances the sensitivity of this hybrid nanostructure based device. If the volume is taken into account, it is deduced that higher surface area-to-volume ratio could be obtained based on the smaller average surface area of individual nanosheets. Inspired by the dynamics of crystal growth, the growth of nanostructure is suggested to be governed by minimal total surface free energy of all possible shapes. The surface area has to be minimized in order to minimize the free energy. Therefore, the growth of ZnO nanosheets favors towards spherical-like clusters, as sphere possesses the least surface area for a given volume among all the other geometrical solid shapes.

Table 1. Comparison of ZnO nanostructures on different templates

ZnO	on TiO_2 nanotubes	on Zn foil
Nanosheet		
Average length	0.62 µm	0.87 µm
Average width	0.05 µm	0.12 µm
Average surface area	0.03 pm^2	0.10 pm^2
Cluster		
Average diameter	5.47 µm	6.72 µm
Average surface area	94.11 pm^2	141.87 pm^2
No. of nanosheets per cluster surface area	~3033	~1385

3.2 Composition and structural properties

Noteworthy from FE-SEM images that the growth of ZnO nanosheets has covered the entire TiO_2 nanotubes, however elemental composition of the sample analyzed by EDX as shown in Table 2 reveals the existence of Ti. The high atomic percentage of oxygen suggests that oxygen may couple with Zn and Ti to form ZnO and TiO_2 in the sample.

Table 2. EDX analysis of ZnO nanostructures in TiO_2 nanotubes

Element	Atomic Percentage (%)
Zinc (Zn)	28.51
Oxygen (O)	67.23
Titanium (Ti)	4.27
Total	100.00

The results were further confirmed by XRD measurement to identify the crystalline phases. The samples were calcined at 500 °C in air as this is an ideal temperature to observe anatase and rutile mixed phase. In order to affirm the crystalline phases of the as-prepared nanosheets, crystalline profile ZnO nanosheets incorporated into TiO_2 nanotubes without thermal treatment is included. The XRD patterns of the above-mentioned samples are shown in Fig. 5.

Three discernable Ti peaks located at 38.40°, 40.18° and 52.98°, correspond to (002), (101) and (102) reflections, respectively, were observed in the XRD pattern of as-anodized TiO_2 nanotubes as shown in Fig. 5 (a). When the sample was incorporated with ZnO nanosheets, intensity of all Ti peaks decreased. Other ZnO peaks appeared at 31.67°, 36.15° and 56.51°, are assigned as (100), (101) and (110) reflections, respectively. No trace of Zn was detected, suggesting that the nanosheets were purely ZnO instead of Zn. This reaffirmed the chemical reactions during the formation of ZnO nanosheets proposed earlier. A carbon (C) peak located at 44.51° was observed in all three samples due to the organic additives in electrolyte. Comparing the calcined TiO_2 nanotubes and the as-anodized TiO_2 nanotubes, the intensity of Ti peaks in calcined sample was lower. An anatase TiO_2 peak at 25.03° was indexed to (110) reflection whereas a rutile TiO_2 peak located at 36.14° was assigned to (102) reflection. Given the melting point of Zn element is approximately 420 °C, slight curled up of Zn nanosheets grown on Zn foil sample was noticed when the sample was calcined at 500 °C. Within this limit of melting point, the ZnO layer was easily self-detached from the Zn surface. Under such circumstances, XRD measurements were inapplicable on the sample. Two unknown peaks labelled as 'x' was recorded in the spectra are yet to be further investigated.

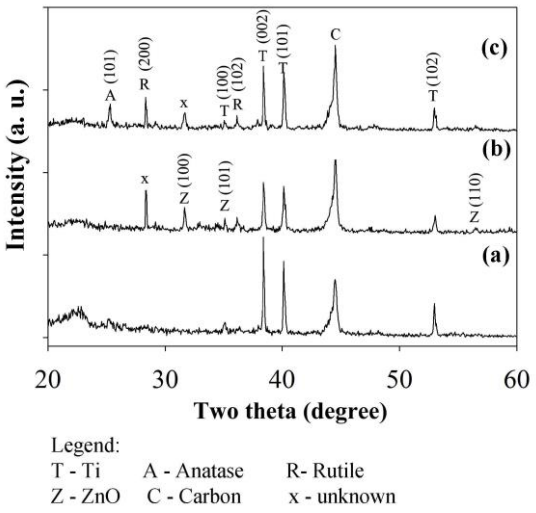

Fig. 5. XRD patterns of (a) as-anodized TiO_2 nanotubes (b) ZnO nanosheets grown on TiO_2 nanotubes and (c) TiO_2 nanotubes calcined at 500 °C.

3.3 Vibrational properties

The vibrational properties of TiO_2 nanotubes and ZnO nanosheets were investigated through Raman spectroscopy. The Raman spectra of the 500 °C-calcined TiO_2 nanotubes has revealed five active modes in anatase phase as shown in Fig. 6 (a). Two dominant peaks 154, 640 cm^{-1} and a shoulder peak 199 cm^{-1} were assigned to the three E_g modes, while 397 and 514 cm^{-1} were both B_{1g} modes. A_{1g} mode in exception was not observed in the samples. Of the two dominant peaks, 154 cm^{-1} peak exhibits a shift by 10 cm^{-1} from the reported E_g mode. This phenomenon was also observed by Beh et al. [17] and Zhang et al. [32] that the first E_g mode was larger than 150 cm^{-1}. The Raman shift phenomenon is more likely to occur among nanostructure, due to the characteristics in various morphologies. Khan investigated ZnO nanostructures of different morphologies including nanowires, nanospheres, flower-like structure and tetrapod structure and reported Raman shifts of -1 to +9 cm^{-1} for different morphologies, as compared to the bulk ZnO [33]. The same thing is believed to occur in TiO_2 nanostructure, but to date the investigation of Raman shifts for TiO_2 structures remains scarce, most probably that, TiO_2 is not easy to diversify into various morphologies, in contrast to ZnO.

Inevitably anatase E_g mode at 144 cm^{-1} coincides with rutile mode at 143 cm^{-1}. In accordance with XRD results of calcined TiO_2 nanotubes sample, the presence of both anatase and rutile peaks allows the possibility for 154 cm^{-1} peak in Fig. 6 (a) to be rutile B_{1g} mode.

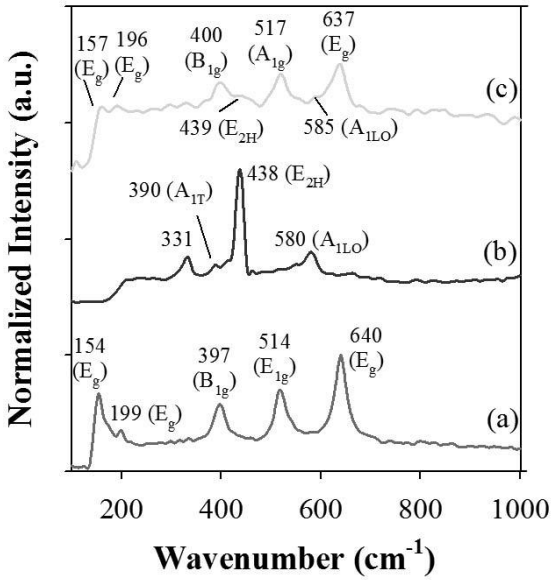

Fig. 6. Raman spectra of (a) TiO_2 nanotubes (b) ZnO nanosheets grown on Zn foil (c) ZnO nanosheets grown on TiO_2 nanotubes, all samples calcined at 500 °C.

On the other hand, wurzite ZnO has six optical modes i.e. $A_1 + 2B_1 + E_1 + 2E_2$. Raman and infrared active A_1 and E_1 modes are polar and may be split into transverse optical (TO) and longitudinal optical (LO) phonons. Both E_2 modes are Raman active only whereas both B_1 modes are inactive or known as silent modes. The contribution of each Raman band in Raman spectrum depends on the scattering cross section of each mode [34, 35].

The Raman spectrum of ZnO nanosheets grown on Zn is shown in Fg. 6 (b). A dominant peak located at 438 cm^{-1} was assigned to E_{2H} mode. A 437–440 cm^{-1} peak has appeared as dominant peak of ZnO thin film and nanostructure in several works [2, 7]. Other peaks observed in the spectrum 390 and 580 cm^{-1}, are assigned to A_{1T} and $A_{1(LO)}$ mode, respectively. Meanwhile a lower peak at 331 cm^{-1} is assigned to $E_{2H} - E_{2L}$ [2].

Raman spectrum of the ZnO nanosheets grown on TiO_2 nanotubes is given in figure 6 (c). Overall, a decrease in peak intensity was observed in all peaks, specifically the intensity of first two TiO_2 E_g modes has experienced a gradual decrement. The 514 cm^{-1} B_{1g} mode was replaced by 517 cm^{-1} A_{1g} mode, summing up three E_g modes, a B_{1g} mode and an A_{1g} mode. Peak broadening phenomenon was observed in the three relatively high intensity peaks and two shoulder peaks arose at 439 and 585 cm^{-1}. In comparison to the nanosheets grown on Zn, the shoulder peaks were assigned to ZnO optical modes E_{2H} and $A_{1(LO)}$, respectively. Hence the existence of these two shoulder peaks clarified the structure of ZnO and this result is consistent with the XRD result.

4. Conclusion

Overall, ZnO nanosheets were successfully deposited on highly ordered TiO_2 nanotubes arrays in ethanolic $Zn(NO_3)_2$ electrolyte. Low applied potential, short anodization time and no extreme temperature are the conditons to synthesis such ZnO nanosheets. The growth preference of ZnO nanosheets in cluster instead of individual sheets was related to the minimum surface energy, whereby near spherical cluster possesses the miminal surface area. The average sizes of cluster as well as nanosheet grown on TiO_2 nanotubes appeared to be smaller than that on Zn foil. The presence of Zn, O and Ti in the sample was confirmed by EDX results and the crystalline phases of TiO_2 nanotubes and ZnO nanosheets were determined by XRD. Raman measurement agreed with XRD results with TiO_2 nanotubes sample showed five TiO_2 active modes and ZnO nanosheets on TiO_2 nanotubes showing two ZnO active modes in raman phase.

Throughout the discussion, the ZnO nanosheets grown on Zn foil sample was served as a comparison sample. XRD and Raman results have shown that the ZnO nanosheets grown on TiO_2 nanotubes has similar characteristics with the nanosheets grown on Zn foil. The nanosheets grown on Zn foil were easily self-detached and turned into powder form, hence careful handling

procedures were required. An advantage of using TiO_2 nanotubes template is that these procedures were not needed.

Acknowledgment

This work was supported by Universiti Sains Malaysia (USM) Exploratory Research Grant Scheme 203/PFIZIK/6730096. The first author acknowledges Ministry of Education Malaysia for MyPhD scholarship.

References

[1] S. Otani, J. Katayama, H. Umemoto, M. Matsuoka, J. Electrochem. Soc. **153**, 551 (2006).
[2] Y. J. Xing, Z. H. Xi, Z. Q. Xue, X. D. Xhang, J. H. Song, R. M. Wang, J. Xu, Y. Song, S. L. Zhang, D. P. Yu, Appl. Phys. Lett. **83**, 1681 (2003).
[3] Y. Li, G. W. Meng, L. D. Zhang, F. Phillipp, Appl. Phys. Lett. **76**, 2011 (2000).
[4] H. W. Kim, H. S. Kim, H. G. Na, J. C. Yang, D. Y. Kim, J. Alloy. Compd., **504**, 217 (2010).
[5] Z. Li, Y. Xiong, Y. Xie, Nanotechnology **16**, 2303 (2005).
[6] B. Cao, W. Cai, H. Zeng, Appl. Phys. Lett. **88**, 161101 (2006).
[7] R. Zhang, P.-G.-Yin, N. Wang, L. Guo, Solid State Sci. **11**, 865 (2009).
[8] V. A. L. Roy, A. B. Djuristic, W. K. Chen, J. Gao, H. F. Lui, C. Surya, Appl. Phys. Lett. **82**, 141 (2003).
[9] J. H. Yang, J. H. Zheng, H. J. Zhai, L. L. Yang, Cyrst. Res. Technol. **44**, 87 (2009).
[10] K. H. Yeo, L. K. The, C. C. Wong, J. Cryst. Growth **287**, 180 (2006).
[11] S. Y. Bae, H. W. Seo, H. C. Choi, J. Park, J. Park, J. Phys. Chem. B **108**, 12318 (2004).
[12] G. Wu, J. Wang, D. F. Thomas, A. Chan, Langmuir **24**, 3503 (2008).
[13] Z. R. Tian, J. A. Voigt, J. Liu, B. Mckenzie, H. Xu, J. Am. Chem. Soc **125**, 12384 (2003).
[14] S. E. John, S. K. Mohapatra, M. Misra, Langmuir **25**, 8240 (2009).
[15] Y. Lei, L. D. Zhang, G. W. Meng, G. H. Li, X. Y. Zhang, C. H. Liang, W. Chen, S. X. Wang, Appl. Phys. Lett. **76**, 1125 (2001).
[16] S. M. H. Hejazi, F. Majidi, M. P. Tavandashti, M. Ranjbar, Mater. Sci. Semicon. Proc. **13**, 267 (2010).
[17] K. P. Beh, F. K. Yam, S. S. Tneh, Z. Hassan, Appl. Surf. Sci. **257**, 4706 (2011).
[18] J. Zhao, C. Jia, H. Duan, H. Li, E. Xie, J. Alloy. Compd. **461**, 447 (2008).
[19] S. J. Kim, J. Choi, Electrochem. Commun. 10, 175 (2008).
[20] F. R. Cummings, L. J. Le Roux, M. K. Mathe, D. Knoesen, Mater. Chem. Phys. **124**, 234 (2010).
[21] F. K. Yam, K. P. Beh, S. W. Ng, Z. Hassan, Thin Solid Films **520**, 807 (2011).
[22] J. M. Macak, H. Tsuchiya, S. Bergerm, S. Bauer, S. Fujimoto, P. Schmuki, Chem. Phys. Lett. **428**, 421 (2006).
[23] B.-Y. Yu, A. Tsai, S.-P. Tsai, K.-T. Wong, Y. Yang, C. Chu, J.-J. Shyue, Nanotechnology **19**, 255202 (2008).
[24] L. Shi, H. Shen, L. Jiang, X. Lin, Mater. Lett. **61**, 4735 (2007).
[25] L. Xu, H. Shen, X. Li, R. Zhu, J. Lumin. **130**, 2123 (2010).
[26] C. W. Zou, X. D. Yan, J. Han, R. Q. Chen, J. M. Bian, E. Haemmerie, W. Gao, Chem. Phys. Lett. **476**, 84 (2009).
[27] P. Xiao, L. Li, Y.-H. Zhang, H.-F. Dai, Y.-Z. Hu, L. Lu, Chin. J. Chem. Phys. **23**, 113 (2010).
[28] Z. Zhang, Y. Yuan, L. Liang, Y. Cheng, G. Shi, L. Jin, J. Hazard. Mater. **158**, 517 (2008).
[29] S. W. Ng, F. K. Yam, Z. Hassan, J. Electrochem. Soc. **159**, D742 (2012).
[30] M. Izaki, T. Omi, J. Electrochem. Soc. **143**, 53 (1996).
[31] S. W. Ng, F. K. Yam, L. L. Low, K. P. Beh, M. F. Mustapha, E. N. Sota, S. S. Tneh, Z. Hassan, Optoelectron. Adv. Mater. – Rapid Comm., **5**, 89 (2011).
[32] W. F. Zhang, Y. L. He, M. S. Zhang, Z. Yin, Q. Chen, J. Phys. D: Appl. Phys. **33**, 912 (2000).
[33] A. Khan, J. Pak. Mater. Soc. **4**, 5 (2010).
[34] T. C. Damen, S. P. S. Porto, B. Tell, Phys. Rev. **142**, 570 (1966).
[35] X. Zhang, Y. Liu, S. Chen, J. Raman Spectrosc. **36**, 1101 (2005).

*Corresponding author: sw.ng@live.com